Research Square

Preprints are preliminary reports that have not undergone peer review.
They should not be considered conclusive, used to inform clinical practice,
or referenced by the media as validated information.

Temporal and spatial changes in the risk of concurrent low cassava yield and wet conditions across Nigeria under global warming

Amit Kumar Srivastava

AmitKumar.Srivastava@zalf.de

Leibniz Centre for Agricultural Landscape Research (ZALF)

Krishnagopal Halder

Leibniz Centre for Agricultural Landscape Research (ZALF)

Ruxin Zhao

National Institute of Natural Hazards, Ministry of Emergency Management of China

Guoqing Lei

Wuhan University

Karam Alsafadi

Xiamen University

Kaushik Muduchuru

Leibniz Centre for Agricultural Landscape Research (ZALF)

Luis Alfredo Pires Barbosa

Leibniz Centre for Agricultural Landscape Research (ZALF)

Kazi Jahidur Rahaman

Leibniz Centre for Agricultural Landscape Research (ZALF)

Manmeet Singh

Western Kentucky University

Wenzhi Zeng

Hohai University

Jaber Rahimi

Pioneer Center Land-CRAFT, Aarhus University

Seyed-Ali Hosseini-Yekani

Leibniz Centre for Agricultural Landscape Research (ZALF)

M. Habib Ur-Rahman

University of Göttingen

Michael Maerker

Leibniz Centre for Agricultural Landscape Research (ZALF)

Thomas Gaiser

University of Bonn
Huu Thuy Nguyen
University of Bonn
Dominik Behrend
University of Bonn
Gang Zhao
Northwest A&F University
Frank Ewert
Leibniz Centre for Agricultural Landscape Research (ZALF)

Article

Keywords: compound climate hazard, crop vulnerability, yield projections, climate adaptation, food security

Posted Date: November 12th, 2026

DOI: https://doi.org/10.21203/rs.3.rs-10844887/v1

License: This work is licensed under a Creative Commons Attribution 4.0 International License.
Read Full License

Additional Declarations: No competing interests reported.

Temporal and spatial changes in the risk of concurrent low cassava yield and wet conditions across Nigeria under global warming

Amit Kumar Srivastava[1*], Krishnagopal Halder[1], Ruxin Zhao[2,3], Guoqing Lei[4], Karam Alsafadi[5], Kaushik Muduchuru[1], Luis Alfredo Pires Barbosa[1], Kazi Jahidur Rahaman[1], Manmeet Singh[6], Wenzhi Zeng[7,8,9], Jaber Rahimi[10,11], Seyed-Ali Hosseini-Yekani[1], M. Habib Ur-Rahman[12], Michael Maerker[1], Thomas Gaiser[13], Huu Thuy Nguyen[13], Dominik Behrend[13], Gang Zhao[14], Frank Ewert[1,13]

[1]Leibniz Centre for Agricultural Landscape Research (ZALF), Eberswalder Str. 84, 15374, Müncheberg, Germany
[2]National Institute of Natural Hazards, Ministry of Emergency Management of China, Beijing 100085, China
[3]Key Laboratory of Compound and Chained Natural Hazards Dynamics, Ministry of Emergency Management of China, Beijing 100085, China
[4]State Key Laboratory of Water Resources Engineering and Management, Wuhan University, Wuhan, China
[5]Key Laboratory of the Ministry of Education for Coastal and Wetland Ecosystems, College of Environment and Ecology, Xiamen University, Xiamen, Fujian 361102, China
[6]Earth, Environmental and Atmospheric Sciences, Western Kentucky University, Bowling Green, KY, United States of America
[7]College of Agricultural Science and Engineering, Hohai University, Nanjing, 210098, China
[8]Key Laboratory of Agricultural Low-Altitude Technology Innovation and Integration, Ministry of Agriculture and Rural Affairs, Nanjing 211100, China
[9]Jiangsu Province Engineering Research Center for Agricultural Soil–Water Efficient Utilization, Carbon Sequestration and Emission Reduction, Nanjing 211100, China
[10]Pioneer Center Land-CRAFT, Department of Agroecology, Aarhus University, Aarhus, Denmark
[11]Institute of Meteorology and Climate Research, Atmospheric Environmental Research (IMK-IFU), Karlsruhe Institute of Technology (KIT), Garmisch-Partenkirchen, Germany
[12]Department of Crop Sciences, Tropical Plant Production and Agricultural Systems Modelling (TROPAGS), Georg-August-University of Göttingen,
[13]Institute of Crop Science and Resource Conservation, University of Bonn, Bonn, 53115, Germany
[14]State Key Laboratory of Soil Erosion and Dryland Farming on the Loess Plateau, College of Soil and Water Conservation Science and Engineering, Northwest A&F University, Yangling, Shaanxi 712100, China

Corresponding Author: Dr. Amit Kumar Srivastava

Leibniz Centre for Agricultural Landscape Research (ZALF),
Eberswalder Str. 84, 15374, Müncheberg, Germany
Email: AmitKumar.Srivastava@zalf.de
Phone: +49 15171288272

Abstract

Cassava is a critical calorie source for millions, and Nigeria is its largest producer, yet climate-driven production risks remain poorly quantified. Using a process-based crop model (SIMPLACE-LINTUL5) driven by ERA5-Land and four CMIP6 climate models, we simulated cassava yields across Nigeria's seven agro-ecological zones for 1995–2013 and under SSP2-4.5 and SSP5-8.5 through 2100. Yield anomalies were combined with the Standardized Precipitation Evapotranspiration Index (SPEI) in a Frank-copula framework to quantify the compound hazard of concurrent low-yield and wet growing-season conditions.

Across all zones, SPEI and yield anomalies were negatively associated (Kendall's $\tau = -0.10$ to -0.32), identifying excess-water stress, rather than drought, as the dominant hydroclimatic constraint in humid zones. Causal analysis confirmed wet-stress sensitivity as a historical signal but identified warming as the primary driver of projected declines: the joint hazard intensifies mainly because rising temperature lowers the yield baseline.

Negligible early in the century, the hazard emerged around 2059–2075 and rose sharply thereafter ($\tau = +0.64$ to $+0.96$), reaching probabilities of 0.13–0.64 during 2071–2100. Assuming constant harvested area, late-century losses could produce a cassava deficit of up to 7.8 Mt annually under high emissions, equivalent to the dietary energy needs of roughly 12 million people.

Keywords: compound climate hazard, crop vulnerability, yield projections, climate adaptation, food security

1. Introduction

Agricultural production is increasingly exposed to hydro-climatic variability and extremes, with drought posing a significant threat to global food security[1]. However, drought remains one of the least comprehensively understood natural hazards, with its impacts varying substantially across space and time[2]. The impacts of agricultural drought, defined as soil moisture depletion below the optimal threshold required for plant growth, depend on the timing, intensity, spatial extent, and persistence of moisture deficits, particularly their coincidence with periods of high crop water demand[3]. Anthropogenic climate change is further intensifying hydro-climatic extremes through rising temperatures and changing precipitation regimes[4], posing increasing risks to staple crops such as cassava. Cassava provides a major source of dietary energy for approximately 800 million people, primarily across Latin America, Asia, and sub-Saharan Africa[5]. Ranked third among calorie-providing staples in the tropics, after rice and maize, cassava is predominantly cultivated by smallholder farmers in the tropical belt (30°N–30°S) across diverse agro-ecological zones[6]. Although it tolerates a broad range of environmental conditions, optimal productivity is generally achieved at temperatures of 25–27°C and annual rainfall of 1,200–1,500 mm[7].

Nigeria, the world's leading cassava producer, has a substantial yield gap, with national yields of approximately 8.76 t ha^{-1} in the late 2010s —well below the yields achieved in major producing countries such as India (34.2 t ha^{-1}) and Laos (32.1 t ha^{-1}), and lower than the global average of 11.1 t ha^{-1}[7]. The predominance of rainfed cultivation further exposes Nigerian cassava production to climatic variability[8]. Moreover, Nigeria spans a broad hydro-climatic gradient, extending from the arid Sahelian north to the humid south, suggesting that the dominant climatic constraints on cassava productivity may vary considerably among agro-ecological zones[9]. Quantifying and projecting these hydro-climatic risks is therefore essential for effective adaptation planning.

A major challenge in assessing hydro-climatic impacts on cassava is the multi-variable nature of drought and the complexity of simultaneous shifts in agronomic and environmental factors[3]. Existing drought indices, including the Standardized Precipitation Index (SPI), Standardized Precipitation Evapotranspiration Index (SPEI), and soil moisture indices, are primarily designed to characterise water deficit[10,11]. However, in humid environments, excess water may impose an equally important or even greater constraint on the productivity of waterlogging-sensitive crops such as cassava[12]. Whether cassava yield is primarily limited by anomalously dry or wet conditions is therefore an empirical question requiring a sign-agnostic analytical framework.

Furthermore, climate-related production risk increasingly arises from compound hazard events in which multiple stressors co-occur, while the probability of their joint occurrence may be underestimated when individual drivers are analysed in isolation[13]. Copula-based joint modelling is well suited to this challenge because it explicitly captures multivariate dependence, accommodates nonlinear associations, and enables intuitive estimates of joint probabilities and return periods[14].

Accordingly, this study employs a bivariate Frank-copula framework to couple a standardised hydro-climatic stress index with cassava yield anomalies across Nigeria's agro-ecological zones, allowing the direction of the hydro-climatic association as an analytical

outcome rather than an a priori assumption. Three objectives are addressed: (1) characterising the bivariate dependence between the Standardized Precipitation Evapotranspiration Drought Index (SPEI) and simulated cassava yield in each zone; (2) quantifying the joint exceedance hazard of concurrent low-yield and hydro-climatically adverse growing seasons; and (3) projecting the spatio-temporal evolution of this compound hazard through 2100 under SSP2-4.5 and SSP5-8.5 emission scenarios. By integrating climate projections, process-based crop simulation, and copula-based risk analysis, this study delivers zone-specific, decision-relevant estimates of climate-driven cassava production risk for evidence-based adaptation planning in Nigeria.

2. Methods

2.1. Data and materials

Daily climate data for 1995–2024, including solar radiation (MJ m^{-2} day^{-1}), precipitation (mm), and minimum and maximum temperatures (°C), were obtained from the ERA5-Land offline land-surface reanalysis of the European Centre for Medium-Range Weather Forecasts[15]. State-level cassava yield data (kg ha^{-1}) for 1995–2014 were obtained from the International Institute of Tropical Agriculture (IITA), Ibadan, Nigeria, for 30 of Nigeria's 36 states and the Federal Capital Territory (FCT). We excluded seven administrative units because of missing or inconsistent yield records. Although climate data were available through 2024 and observed yields through 2014, the historical joint-risk analysis was restricted to 1995–2013, the period for which a consistent SPEI–yield record was available across all agro-ecological zones. The projection period began in 2016, the first year providing complete cassava SPEI–yield coverage across all seven zones; 2015 was excluded because it provided only partial, short-season coverage in several northern states. As no significant yield trend was detected during 1995–2013, detrending was not applied.

Cassava sowing dates were obtained from the FAO crop calendar[16]. Net nitrogen and phosphorus were applied at 20 and 5 kg ha^{-1}, respectively, following recommendations from the Federal Ministry of Agriculture and Rural Development[17]. Because information on the spatial distribution of cassava varieties is limited, the most popular cassava variety, TME419, was simulated across all 37 administrative units (https://wikifarmer.com/library/en/article/cassava-varieties). Soil properties, including sand, silt, clay, gravel, cation exchange capacity, pH, organic carbon, and bulk density, were obtained from the 1 × 1 km African Soil Property Maps (https://www.isric.org/ projects/soil-property-maps-africa-1-km-resolution). Other soil input parameters required in the crop model, such as soil water at field capacity, wilting point, saturation point, and Van-Genuchten parameter, were also estimated according to [18].

We obtained future climate projections from the NASA Earth Exchange Global Daily Downscaled Projections (NEX-GDDP-CMIP6), which are bias-corrected and spatially downscaled to 0.25° (~25 km) using the Bias-Correction Spatial Disaggregation (BCSD) method[19]. We selected climate models based on their spread across the spectrum of Equilibrium Climate Sensitivity (ECS) and Transient Climate Response (TCR). The four retained CMIP6 global climate models were CanESM5 [20](CCCma, Canada), MIROC-ES2L[21] (MIROC, Japan), MPI-ESM1-2-LR[22] (MPI-M, Germany), and NorESM2-MM[23] (NCC, Norway). These models

include low, moderate and high sensitivity ranges which capture structural model uncertainty. CanESM5 represents a high warming response with ECS of 5.6°C which is indicative of aggressive feedback loops in clouds and radiative forcing. This provides an upper bound for the land-atmosphere interactions over tropical regions. Meanwhile, MPI-ESM1-2-LR represents a moderate response with an ECS of 3.0 K. Completing the ensemble, MIROC-ES2L and NorESM2-MM represent lower-to-moderate sensitivity pathways with ECS values of 2.7 K and 2.5 K, respectively. The MPI-ESM1-2-LR model demonstrates superior skill in capturing the atmospheric and oceanic drivers of the West African Monsoon pertinent to Nigerian precipitation patterns[24]. The other models in the ensemble also sufficiently resolve regional processes such as SST modulation of the inland moisture fluxes and jet-driven mesoscale convective organisation[25]. Each model provides daily precipitation, radiation, and temperature projections under the SSP2-4.5 and SSP5-8.5 scenarios for 2016–2100. The ensemble mean of the four models was used for the main analysis, while inter-model spread represented model structure uncertainty.

2.2. Cassava yield simulations and validation

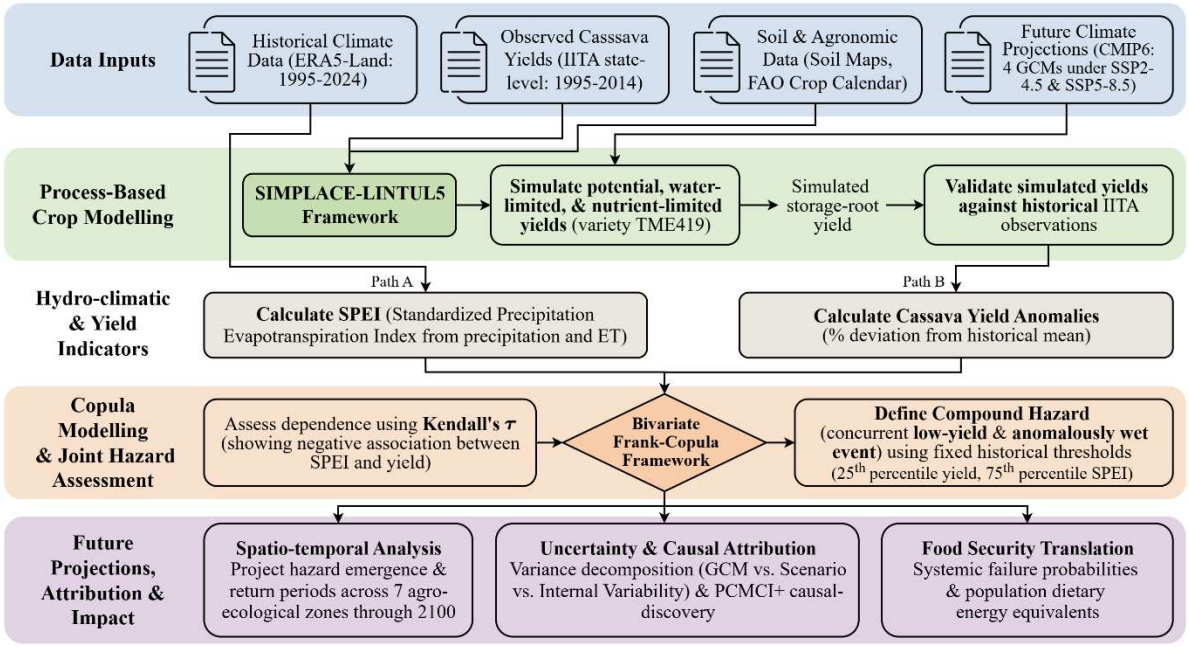
Cassava storage-root yield and above-ground biomass were simulated using the LINTUL5 crop model within the SIMPLACE (Scientific Impact Assessment and Modelling Platform for Advanced Crop and Ecosystem Management) framework[26,27]. LINTUL5 simulates potential, water-limited, and nutrient-limited yields. Potential yield is driven only by solar radiation and temperature under optimal conditions[28], whereas water-limited yield additionally accounts for soil water availability and water stress[29]. Nutrient-limited simulations consider water, NPK, temperature, and radiation stresses, which jointly constrain biomass accumulation, root growth, and yield[30].

Biomass production is calculated from intercepted radiation and radiation-use efficiency following Lambert–Beer's law[31]. The resulting biomass is partitioned among leaves, stems, storage organs, and roots according to development-stage-dependent coefficients[32]. Crop phenology is simulated by accumulating thermal time above a defined base temperature, and the growth cycle is defined from emergence to physiological maturity[33]. Soil water dynamics are simulated using the SLIM conceptual soil-water balance model, which represents the soil using a variable number of layers[34].

We used the default LINTUL5 cassava parameterisation as the starting point for developing an optimised parameter set for the TME419 variety. We obtained plausible parameter ranges from the literature[35] and used systematic sampling across the parameter space to identify the parameter set with the smallest mean residual error based on simulated yield and phenology observations. **Supplementary table S1** provides the final parameterisation, and **Figure 1** shows a schematic of the entire workflow. Analyses were performed at the level of Nigeria's seven agro-ecological zones—Sahel Savanna, Sudan Savanna, Northern Guinea Savanna, Southern Guinea Savanna, Derived Savanna, Mid-Altitude and Humid Forest—which partition the country along its south-to-north rainfall, temperature and growing-season gradients[7]. We aggregated the state-level cassava simulations and the corresponding SPEI series into these zones before the dependence and copula analysis.

The cassava simulations were previously evaluated against observed state-level yields across 30 Nigerian states during 1995–2014, showing close agreement ($R^2 = 0.89$, RMSE =

194 0.40–0.47 t ha⁻¹); mean overestimation ≈ 5.5%[36]. Consistent with this evaluation, the state-
195 mean yields used in the present analysis showed strong agreement with observations ($R^2 =$
196 0.89, RRMSE = 11.4%, Willmott's $d = 0.96$ and mean bias = +8.5%), supporting their use in
197 the subsequent analysis.



198
199 **Figure 1.** Schematic diagram of the entire workflow. The analytical framework integrates historical
200 observations and future CMIP6 climate projections with the SIMPLACE-LINTUL5 process-based crop
201 model to simulate cassava yield responses. Simulated yields and climate data are transformed into
202 cassava yield anomalies and the Standardized Precipitation Evapotranspiration Index (SPEI),
203 respectively, and the two are coupled using a bivariate Frank copula model. The final phase translates
204 this joint hazard framework into an integrated risk assessment that evaluates spatio-temporal hazard
205 projections, projection uncertainty, causal attribution, and food security impacts across Nigeria's agro-
206 ecological zones.

207 **2.3. Hydro-climatic indicators, yield anomalies, and dependence assessment**

208 This study evaluates the relationship between hydro-climatic indicators and cassava yield by
209 deriving two primary variables for each agro-ecological zone: the Standardized Precipitation
210 Evapotranspiration Drought Index (SPEI) and the cassava yield anomaly. SPEI is a signed
211 hydro-climatic stress index, derived from the accumulated water deficit (D_k) over a (w)-month
212 accumulation window corresponding to the cassava growing season[37,38]. D_k is the difference
213 between precipitation (Pre_i) and actual (ETa_i) evapotranspiration:

$$D_k = \sum_{i=k-w+1}^{k} (Pre_i - ETa_i) \quad (1)$$

214 where k denotes the final month of the (w)-month accumulation period. The resulting values
215 of D_k were fitted to an appropriate probability distribution with cumulative distribution
216 function (CDF) F and subsequently transformed to a dimensionless standard-normal scale:

$$SPEI_k = \Phi^{-1}\big(F(D_k)\big) \quad (2)$$

where Φ^{-1} is the inverse CDF of the standard normal distribution. The negative SPEI values indicate drier-than-normal conditions, while positive values indicate wetter-than-normal conditions.

For each agro-ecological zone and year, the cassava yield anomaly (y) was calculated as the percentage deviation of the simulated yield (Y) from the historical reference-period mean ($\bar{Y}_{ref}$):

$$y = 100 \times \frac{Y - \bar{Y}_{ref}}{\bar{Y}_{ref}} \tag{3}$$

The direction and strength of the observed monotonic dependence between SPEI and cassava yield anomaly were initially characterized using Kendall's rank correlation coefficient (τ):

$$\tau = \frac{n_c - n_d}{\frac{1}{2}n(n-1)} \tag{4}$$

where n_c and n_d are the numbers of concordant and discordant observation pairs, respectively, among the total n observations. The estimated Kendall's τ was subsequently used to parameterize the copula model described in the following section.

2.4. Copula modelling, joint hazard, and systemic risk

For each agro-ecological zone, the joint dependence structure between SPEI (S) and cassava yield anomaly (y) was modelled using a bivariate copula. The marginal distributions of SPEI and yield anomaly were assumed to be normal and transformed into uniform probabilities on the interval ($[0, 1]$), using their respective CDFs:

$$u = F_S(s) = \Phi\left(\frac{s - \mu_S}{\sigma_S}\right), \qquad v = F_y(y) = \Phi\left(\frac{y - \mu_y}{\sigma_y}\right) \tag{5}$$

where s and y denote observed values of SPEI and yield anomaly, respectively; Φ is the standard-normal CDF; and μ and σ denote the mean and standard deviation of each variable over the study period.

Because SPEI and cassava yield anomaly exhibit negative dependence, standard Clayton and Gumbel Archimedean copulas[39], which represent only positive dependence with asymmetric tail dependence, were excluded. The Frank copula was selected because it accommodates the full range of symmetric dependence and has no tail dependence. The suitability of the Frank copula was assessed against alternative copula families using the Akaike information criterion (AIC), Bayesian information criterion (BIC), and the Cramér–von Mises goodness-of-fit statistic[40]. The Frank copula is defined as:

$$C(u, v; \theta) = -\frac{1}{\theta}\ln\left[1 + \frac{(\exp(-\theta u) - 1)(\exp(-\theta v) - 1)}{\exp(-\theta) - 1}\right] \tag{6}$$

where u and v are the marginal uniform probabilities and θ is the copula dependence parameter.

The dependence parameter (θ) was estimated numerically from the Kendall's τ value calculated in Section 2.3 using the following relationship between Kendall's τ and the Frank copula parameter, where $D_1(\theta)$ represents the first-order Debye function:

$$\tau = 1 - \frac{4}{\theta}[1 - D_1(\theta)], \qquad D_1(\theta) = \frac{1}{\theta}\int_0^{\theta} \frac{t}{\exp(t) - 1}\, dt \tag{7}$$

The compound hazard (H) was defined as the probability (P) of a concurrent low-yield and anomalously wet event. The low-yield threshold (y_{low}) was fixed at the 25th percentile of the historical reference period (1995–2013), whereas the wet-condition threshold (S_{high}) was fixed at the corresponding 75th percentile of SPEI. By using these fixed historical thresholds to assess changes in the compound hazard over time, the return period of the event was calculated as $T = 1/H$ (where H = 0.2 ≈ once in five years).

$$H = P\big(Y < y_{\text{low}}, S > S_{\text{high}}\big) = F_Y(y_{\text{low}}) - C\big(F_Y(y_{\text{low}}), F_S\big(S_{\text{high}}\big); \theta\big) \tag{8}$$

To assess systemic risk across the seven agro-ecological zones, the expected number of zones affected by the compound event in year t was calculated as:

$$E[N(t)] = \sum_{z=1}^{7} H_z\,(t) \tag{9}$$

where $N(t)$ is the number of agro-ecological zones experiencing a low-yield-wet event in year t, and $H_z(t)$ is the estimated compound-hazard probability for zone (z). The probability that at least k zones experience the compound hazard in the same year was evaluated under two dependence assumptions. The k-th largest zone-specific hazard was used as the comonotonic upper bound, representing perfect positive dependence among zones, whereas an independence-based Poisson–binomial model was used as an independence benchmark.

2.5. Temporal trends, emergence, uncertainty, and causal attribution

Temporal trends in annual compound hazard over 2016–2100 were assessed using the non-parametric Mann–Kendall test (S) and Sen's slope (β). For annual hazard values x_i observed over n years, the two statistics were calculated as:

$$S = \sum_{i<j} \operatorname{sgn}\big(x_j - x_i\big), \qquad \beta = \operatorname{median}_{i<j}\left(\frac{x_j - x_i}{j - i}\right) \tag{10}$$

where i and j denote the earlier and later years, respectively. Positive and negative values of S and β indicate increasing and decreasing trends, respectively.

The time of emergence (ToE) was defined as the first year when the forced hazard signal permanently exceeded one standard deviation of internal variability (σ_{int}). The signal-to-noise ratio (SNR) was calculated as:

$$SNR(t) = \frac{|H(t) - \bar{H}_{hist}|}{\sigma_{int}}; \quad ToE = \min\{t: SNR(t') > 1 \; \forall t' \geq t\} \tag{11}$$

Following [41], projection uncertainty was partitioned into climate-model uncertainty (V_M), emission-scenario uncertainty (V_S), and internal variability (V_I). The total variance (V_T) was calculated as the sum of these components. Each model–scenario hazard trajectory (h) was smoothed using a fourth-order polynomial ($\hat{h}$) and the variance components were calculated as:

$$V_M(t) = \mathrm{Var}_m\left[\hat{h}_{m\cdot}(t)\right], \quad V_S(t) = \mathrm{Var}_s\left[\hat{h}_{\cdot s}(t)\right], \quad V_I = \left\langle \mathrm{Var}_t\left(h - \hat{h}\right)\right\rangle \tag{12}$$

$$V_T(t) = V_M(t) + V_S(t) + V_I \tag{13}$$

where m, s, t indicate variance across climate models, scenarios, and time, respectively; the dot denotes averaging over the other dimension (i.e., across scenarios for $\hat{h}_{m\cdot}$ and across climate models for $\hat{h}_{\cdot s}$), and $\langle\cdot\rangle$ denotes averaging across all model-scenario trajectories. Using these smoothed hazard trends, the fractional contribution of each uncertainty source was calculated as:

$$f_x(t) = \frac{V_x(t)}{V_T(t)} \tag{14}$$

where x denotes the specific source (model, scenario, or internal variability). The fractions of all three sources add up to one.

To distinguish hydro-climatic effects from coincident long-term trends, cassava yield anomalies and four drivers—SPEI, temperature, solar radiation, and precipitation—were detrended using an 11-year centred moving average. The partial correlation (r) between yield anomaly (Y) and each driver (X), while controlling for the remaining drivers (Z), was calculated as:

$$r_{Y,X\cdot Z} = \mathrm{corr}\left(Y - \hat{Y}(Z),\, X - \hat{X}(Z)\right) \tag{15}$$

where X represents the tested driver and Z represents the other three drivers. $\hat{Y}(Z)$ and $\hat{X}(Z)$ are the linear-regression predictions of Y and X based on Z, respectively. Thus, the residual correlation represents the association between Y and X after accounting for the influence of the other drivers. Additionally, the PCMCI+ [42] causal-discovery algorithm was applied to identify direct causal drivers of the yield anomaly.

2.6. Food-security translation

The late-century national yield anomaly ($\bar{a}$) was translated into tangible food security metrics: a production shortfall (ΔP) and the population equivalent in dietary energy terms (N_p), using FAOSTAT production data, cassava energy content, and the proportion of production allocated for human consumption:

$$\Delta P = \left(\frac{|\bar{a}|}{100}\right) \cdot P_0; \quad N_p = \frac{\Delta P \cdot \varepsilon \cdot \phi}{c \cdot 365} \tag{16}$$

where P_0 is baseline production, ε is the fresh-root energy content ($\varepsilon \approx 1.6$ Mkcal t^{-1}), ϕ is the edible fraction (85%), and c is the average per-capita dietary requirements ($c \approx 2500$ kcal day^{-1}according to [43]). The economic value of the production shortfall was estimated by applying the farm-gate price to ΔP.

3. Results

3.1. Hydro-climatic dependence and emergence of compound low-yield/wet hazard

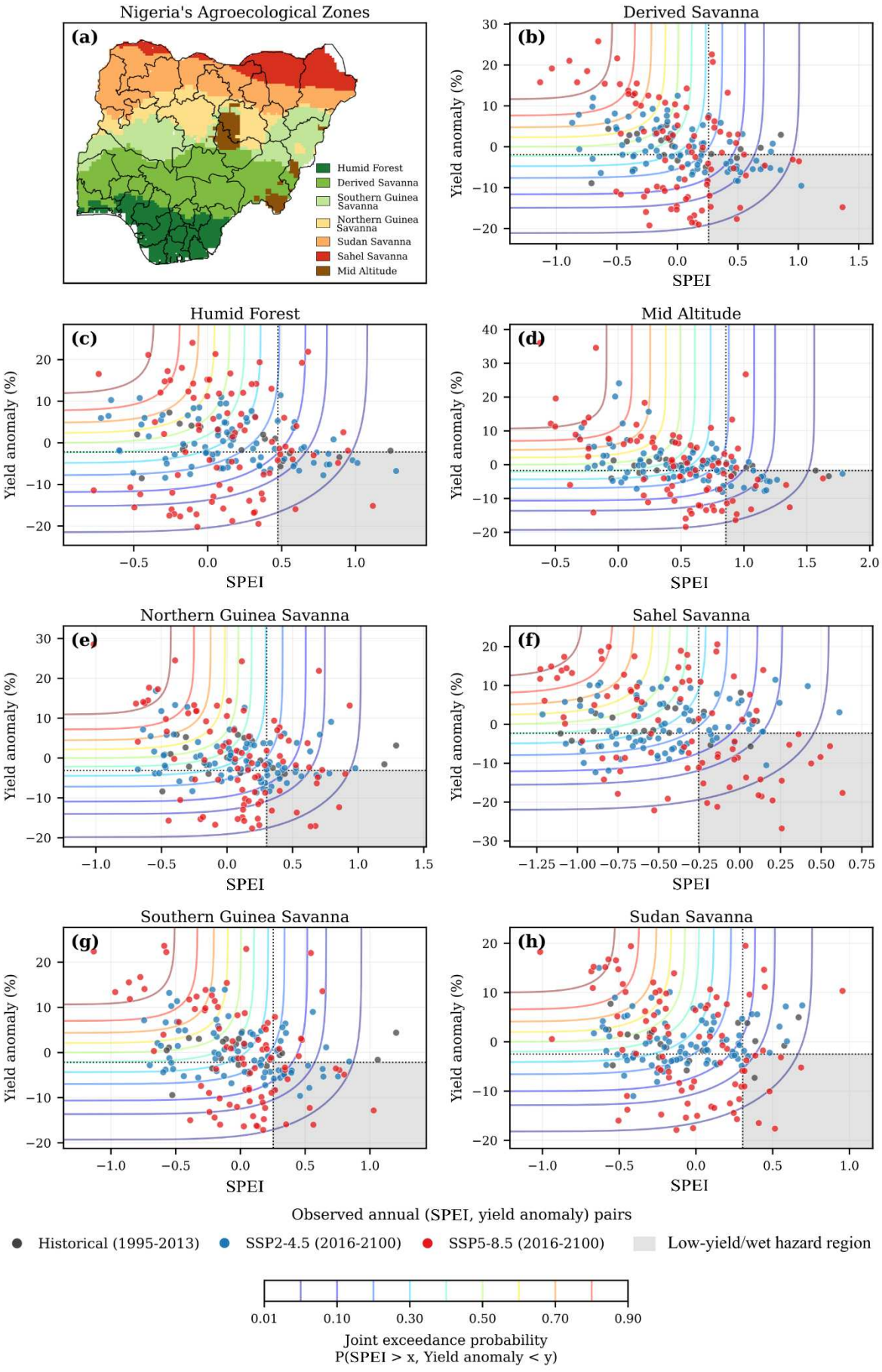
Across all seven agro-ecological zones, SPEI and cassava yield anomaly exhibited an overall negative dependence during 1995-2100, indicating that wetter-than-normal conditions were generally associated with below-normal cassava yields (**Figures 2 and 3a**). This pattern suggests that excess-water stress, rather than drought, is an important hydro-climatic constraint on cassava production in this predominantly humid region. The strength of the dependence varied among zones, with the strongest associations observed in the Mid Altitude (Kendall's $\tau = -0.32, p < 0.001$), Derived Savanna ($\tau = -0.27, p < 0.001$), and Southern Guinea Savanna ($\tau = -0.24, p < 0.001$) zones, and the weakest in the Humid Forest ($\tau = -0.10, p < 0.05$) (**Table 1**). All pooled relationships were statistically significant. Although some scenario-specific relationships were weak or locally positive in the northern zones, the pooled dependence over 1995-2100 remained negative in every zone. A Frank copula was therefore used to represent the moderate, approximately symmetric dependence between SPEI and yield anomaly. The Frank and Gaussian copulas provided statistically indistinguishable fits in six of the seven zones ($|\Delta\text{AIC}|$ and $|\Delta\text{BIC}| < 2$), with the Sahel Savanna as the only exception. The Frank copula also closely reproduced the empirical dependence structure, with Cramér–von Mises goodness-of-fit statistics ranging from 0.02 to 0.05 across zones. The Frank copula was therefore retained for the joint-hazard analysis because of its good empirical fit and analytical tractability; the Gaussian copula produced near-identical hazard estimates.

In the compound hazard analysis, we quantified the probability of concurrent low-yield and wet conditions across the historical baseline (1995–2013), early-century (2016–2040), mid-century (2041–2070), and late-century (2071–2100) periods. Historical hazard values ranged from 0.063 in the Sudan Savanna to 0.138 in the Derived Savanna (**Table 1**), corresponding to return periods of approximately 7.2-15.9 years (**Table 2**). During the early-century period, the hazard declined to near zero in all zones ($H \leq 0.015$) because simulated yields remained 5–16% above the historical baseline, resulting in few years falling below the historical low-yield threshold despite the persistence of wet conditions.

Beyond mid-century, the hazard increased strongly and monotonically in every zone under both scenarios (**Figure 4**). Mann-Kendall statistics ranged from 0.64 to 0.96 ($p < 0.001$) (**Table 1**), with Sen's slopes ranging from 0.02 to 0.11 per decade. A sustained hazard ($H \geq 0.2$) emerged mainly between the 2060s and early 2070s, generally earlier under SSP5-8.5 (2059-2069) than under SSP2-4.5 (2062-2075) (**Figure 3e, f**). By the late-century period, hazard values reached 0.134-0.640 across the affected zones under SSP5-8.5 (**Table 1**), corresponding to concurrent low-yield/wet events occurring every 1.6-7.5 years (**Table 2**). The

spatial pattern of late-century hazard differed markedly between the two emission scenarios (**Figure 3b, c**). The highest late-century hazard occurred in the Sahel Savanna under SSP5-8.5 ($H = 0.640$, approximately one event every 1.6 years), followed by the Northern Guinea Savanna ($H = 0.396$). Under SSP2-4.5, the largest hazards occurred in the Derived Savanna ($H = 0.495$) and Mid Altitude ($H = 0.413$) zones. The Sudan Savanna under SSP2-4.5 was the only exception, remaining close to its historical hazard level ($H = 0.063$).

The two pathways diverged in the late century in a zone-dependent manner. SSP5-8.5 produced substantially higher late-century hazard in the northern savanna zones, particularly the Sahel and Sudan Savannas, whereas SSP2-4.5 produced higher hazards in the wetter southern zones, including the Derived Savanna, Humid Forest, and Southern Guinea Savanna (**Figure 3b-d**). Hazard decomposition showed that the projected decline in the yield distribution was the primary driver of the emerging compound hazard. When the late-century yield distribution was held at its early-century state, the projected increase in hazard was largely eliminated. In contrast, changes in SPEI alone produced only a limited increase in hazard, indicating that wetter conditions mainly amplified risk after low-yield years became more frequent. As a result, by the late-century period, the probability of a low-yield year during wet conditions reached 0.80–1.00 across zones and 0.97–1.00 under SSP5-8.5. Thus, by the end of the century, wet years were projected to be associated with low cassava yields in nearly all cases.


Nigeria's Agroecological Zones
(a)
Humid Forest
Derived Savanna
Southern Guinea Savanna
Northern Guinea Savanna
Sudan Savanna
Sahel Savanna
Mid Altitude
Derived Savanna
(b)
Humid Forest
(c)
Mid Altitude
(d)
Northern Guinea Savanna
(e)
Sahel Savanna
(f)
Southern Guinea Savanna
(g)
Sudan Savanna
(h)
Yield anomaly (%)
SPEI
Observed annual (SPEI, yield anomaly) pairs
Historical (1995-2013)
SSP2-4.5 (2016-2100)
SSP5-8.5 (2016-2100)
Low-yield/wet hazard region
0.01
0.10
0.30
0.50
0.70
0.90
Joint exceedance probability
P(SPEI > x, Yield anomaly < y)

357

Figure 2. (a) Map of Nigeria's Agroecological Zones. Frank-copula joint distribution of SPEI and cassava yield anomaly (%) for the seven agro-ecological zones of Nigeria: (b) Derived Savanna, (c) Humid Forest, (d) Mid Altitude, (e) Northern Guinea Savanna, (f) Sahel Savanna, (g) Southern Guinea Savanna and (h) Sudan Savanna. In panels (b) through (h), the horizontal axis is SPEI (negative = drier than normal) and the vertical axis is the cassava yield anomaly (%). Coloured contours are levels of the survival copula P (yield anomaly < y and SPEI > x), from 0.01 to 0.90 as indicated by the shared colorbar, fitted with a Frank copula on the pooled 1995–2100 record per zone (dependence parameter from the pooled Kendall τ; Gaussian marginals with pooled mean and standard deviation). SPEI and the yield anomaly are the four-GCM ensemble mean (CanESM5, MIROC-ES2L, MPI-ESM1-2-LR, NorESM2-MM). Dotted lines mark the fixed hazard thresholds: historical (1995–2013) 25th-percentile yield anomaly and historical 75th-percentile SPEI, and the shaded lower-right corner is the concurrent low-yield/wet hazard region. Observed annual (SPEI, yield-anomaly) pairs are overlaid for the historical period (dark grey, 1995–2013), SSP2-4.5 (blue, 2016–2100) and SSP5-8.5 (red, 2016–2100); across all seven zones, the future point clouds shift toward the low-yield/wet corner relative to the historical baseline, with the largest displacement under SSP5-8.5.

Table 1. Kendall's τ between SPEI and cassava yield anomaly (1995–2100), historical (1995–2013) joint low-yield/wet hazard, late-century (2071–2100) hazard under SSP2-4.5 / SSP5-8.5, and the Mann-Kendall trend statistic of the 2016–2100 hazard trajectory under SSP5-8.5. Significance levels are $*$ $p < 0.05$, $**$ $p < 0.01$, and $***$ $p < 0.001$.

Zone	SPEI–yield dependence (Kendall's τ)	Historical hazard (1995–2013)	Late-century hazard (2071–2100)SSP2-4.5 / SSP5-8.5	Mann–Kendall trend (2016–2100, SSP5-8.5)
Derived Savanna	−0.27***	0.138	0.495 / 0.316	+0.78***
Humid Forest	−0.10*	0.093	0.378 / 0.134	+0.64***
Mid Altitude	−0.32***	0.134	0.413 / 0.284	+0.82***
Northern Guinea Savanna	−0.21***	0.118	0.354 / 0.396	+0.84***
Sahel Savanna	−0.15**	0.093	0.216 / 0.640	+0.96***
Southern Guinea Savanna	−0.24***	0.135	0.411 / 0.346	+0.82***
Sudan Savanna	−0.13**	0.063	0.063 / 0.215	+0.89***

Table 2. Historical and projected return periods of concurrent low-yield/wet hazard events and the timing of hazard emergence across Nigeria's agro-ecological zones. Return period (RP = 1/H) is shown for the historical baseline (1995–2013) and the late-century period (2071–2100) under SSP2-4.5 and SSP5-8.5. The emergence year corresponds to the first year under SSP5-8.5 when the annual hazard reached and remained above $H \geq 0.2$.

Zone	Historical RP (1995–2013)	Late-century RP (SSP2-4.5)	Late-century RP (SSP5-8.5)	Emergence year (SSP5-8.5)
Derived Savanna	7.2	2.0	3.2	2059
Humid Forest	10.8	2.6	7.5	2063
Mid Altitude	7.5	2.4	3.5	2059
Northern Guinea Savanna	8.5	2.8	2.5	2063
Sahel Savanna	10.8	4.6	1.6	2062
Southern Guinea Savanna	7.4	2.4	2.9	2060

Sudan Savanna	15.9	15.9	4.7	2069

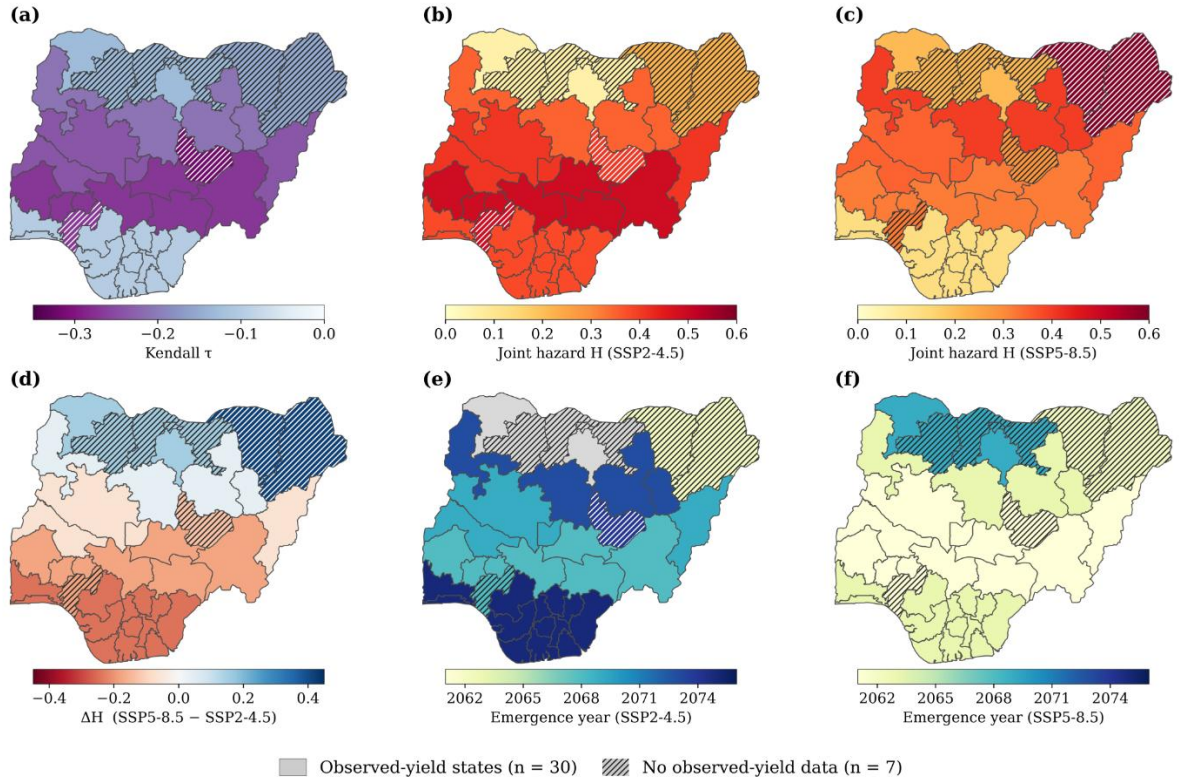


Figure 3. Spatial patterns of cassava low-yield/wet hazard across Nigeria. (a) Kendall's τ between SPEI and cassava yield anomaly, showing negative dependence across all zones, with darker purple indicating stronger wet-stress coupling; (b) ensemble-mean late-century (2071–2100) joint hazard H under SSP2-4.5; (c) the corresponding hazard under SSP5-8.5; (d) scenario contrast, $\Delta H = H_{\mathrm{SSP5-8.5}} - H_{\mathrm{SSP2-4.5}}$, with positive values indicating greater hazard under SSP5-8.5 and negative values indicating greater hazard under SSP2-4.5; (e) year in which H first reaches and sustains ($H \geq 0.2$) under SSP2-4.5; and (f) the corresponding emergence year under SSP5-8.5. Panels (b) and (c), and panels (e) and (f), use the same colour scale for direct comparison.

3.2. Projection uncertainty and time of emergence

The projected increase in compound hazard was evident across all four CMIP6 climate models. In every zone and under both scenarios, all models projected higher late-century hazards than during the early century, and the ensemble-mean late-century signal was approximately twice the inter-model standard deviation (median SNR ~ 2.0; **Figure 4a-g**). The projected increase was therefore not driven by an individual climate model.

Variance decomposition revealed a substantial shift in the sources of uncertainty over time (**Figure 4h**). In the early century, internal variability accounted for about 68% of total uncertainty because the forced hazard signal remained close to zero. As the hazard intensified, internal variability's contribution declined substantially. By the late century, climate-model spread accounted for approximately 54% of the total variance, followed by emission-scenario uncertainty (35%), while internal variability contributed only about 11%. These results indicate that the late-century increase represents a robust forced response, although its magnitude remains sensitive to differences among climate models and, to a lesser extent, future emissions pathways.

The time-of-emergence (ToE) analysis provided further evidence of a mid-century transition. Under SSP2-4.5, the forced signal permanently exceeded one standard deviation of internal variability between 2054 and 2069, although no emergence was detected in the Sudan Savanna. Under SSP5-8.5, emergence occurred between 2057 and 2081. These estimates are consistent with the timing at which hazard first reached and sustained ($H \geq 0.2$), confirming that the increase in compound low-yield/wet risk becomes distinguishable from internal climate variability primarily after the middle of the century.

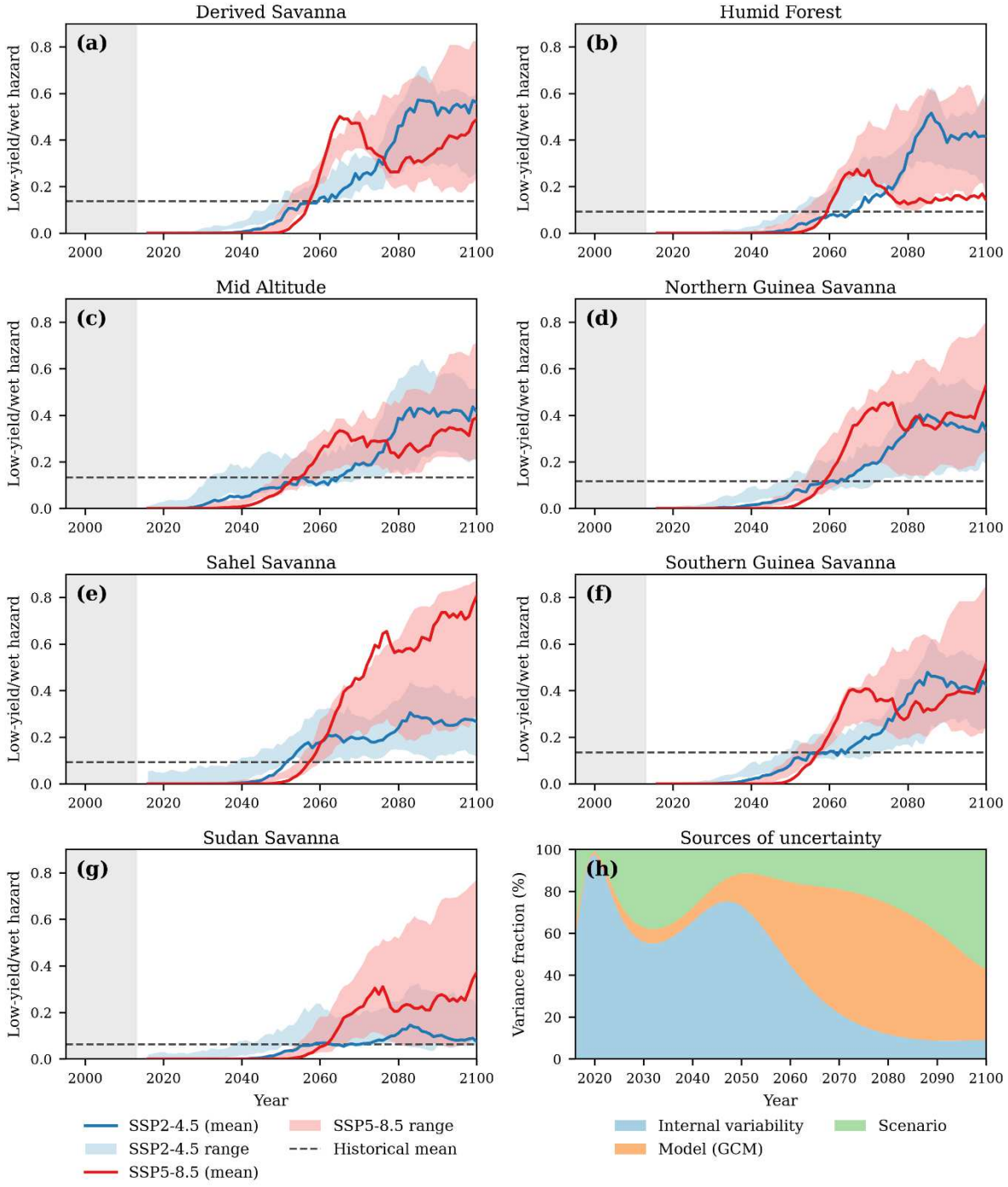


Figure 4. Joint low-yield/wet hazard trajectories across seven Nigerian agro-ecological zones and sources of projection uncertainty. Panels (a)–(g) show the annual joint-hazard probability ($H =$

$P(Y < y_{\text{low}}, S > S_{\text{high}})$ for each zone under SSP2-4.5 (blue) and SSP5-8.5 (red), where y_{low} and S_{high} are the zone-specific historical (1995–2013) 25th-percentile yield anomaly and 75th-percentile SPEI, respectively. H was computed using a Frank copula with a stationary dependence parameter θ (derived from the pooled 1995–2100 Kendall τ) and non-stationary normal marginals whose means follow a 21-year centred moving average of the ensemble-mean projection. Solid lines show the four-GCM ensemble mean; shaded bands span the full inter-GCM range across CanESM5, MIROC-ES2L, MPI-ESM1-2-LR, and NorESM2-MM, computed under common thresholds. The dashed horizontal line marks the historical-period mean hazard; the grey shading covers the 1995–2013 calibration window. Panel (h) shows the Hawkins–Sutton variance decomposition of H for 2016–2100, partitioning total projection uncertainty into contributions from internal variability (blue), climate-model spread (orange), and emission-scenario uncertainty (green).

3.3. Implications for Cassava production and food-security risk

The emerging compound hazard has potentially substantial implications for Nigeria's cassava production and food security. National yield anomalies were positive during the early century, representing a surplus of approximately 6-14% relative to the historical baseline, but subsequently declined to late-century deficits of 4.7% under SSP2-4.5 and 12.5% under SSP5-8.5 (**Figure 5a**). Applying these anomalies to current national cassava production of 60.01 Mt[44] and holding the harvested area constant at approximately 7.8 Mha[45] yields estimated production shortfalls of about 3.0 and 7.8 Mt yr^{-1}, respectively. Using an energy content of 1.6 $Mkcalt^{-1}$ approximately[46], these losses are equivalent to the annual dietary energy requirements of roughly 4 million people under SSP2-4.5 and 12 million people under SSP5-8.5.

Because concurrent low-yield/wet events are projected to become frequent by the end of the century, these losses represent a potentially chronic rather than episodic pressure on the national food supply. At recent farm-gate cassava prices of approximately US$70-130 t^{-1} [47], the projected production shortfalls correspond to an economic loss of roughly US$0.5-1.0 billion per year. These estimates indicate the scale of potential exposure rather than provide a precise forecast because they assume constant harvested area, demand, and management.

The projected risk is also spatially coherent. Yield anomalies were strongly correlated among agro-ecological zones, with a mean pairwise correlation of r = 0.95, indicating that low-yield years are likely to occur simultaneously across large parts of the country rather than remain geographically isolated. Under SSP5-8.5, the expected number of zones concurrently experiencing low-yield/wet conditions increased from near zero historically to approximately 2.5 of seven by 2071-2100 (**Figure 5b**). Accounting for the strong spatial dependence, the probability that at least five zones would be affected simultaneously reached approximately 0.3, equivalent to a national multi-zone event occurring about once every three years. This probability is substantially greater than the approximately 0.05 expected under independent zone failures. The high degree of synchrony limits opportunities for geographic risk pooling and increases the vulnerability of the national cassava supply to widespread climate-related production losses.

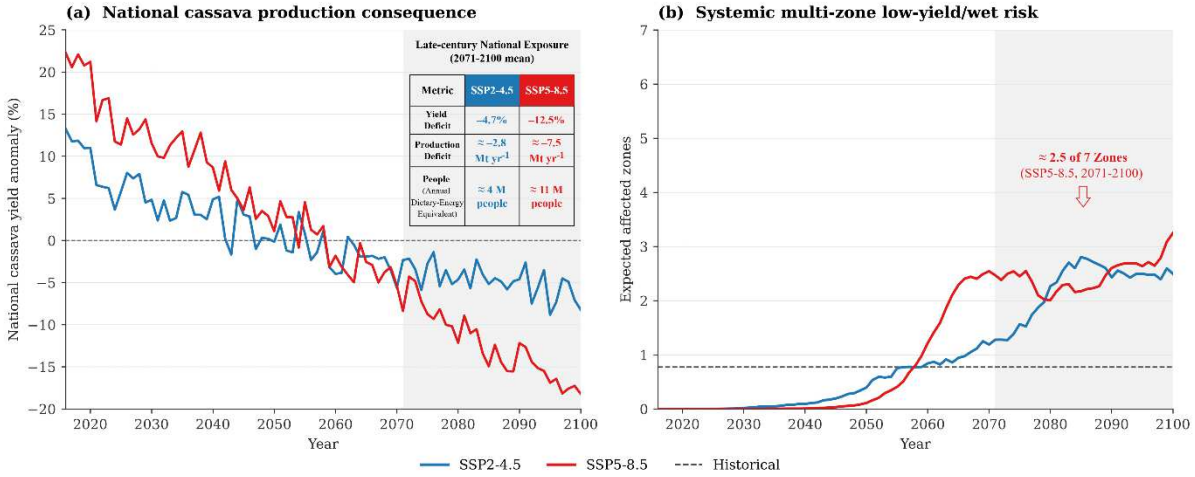


Figure 5. National consequences and systemic multi-zone risk of compound low-yield/wet hazards for Nigeria's cassava production. (a) Projected ensemble-mean national yield anomalies (%) from 2016 to 2100 under SSP2-4.5 (blue line) and SSP5-8.5 (red line) relative to the historical baseline. Early-century projections indicate a yield surplus, which subsequently declines into chronic late-century deficits (2071–2100 mean, grey shading). The inset table quantifies this late-century national exposure, translating percentage deficits into estimated production shortfalls (Mt yr^{-1}) and the equivalent millions of people whose annual dietary energy requirements would be affected, assuming a constant baseline production of 60.01 Mt and a harvested area of 7.8 Mha. (b) The expected number of Nigeria's seven agro-ecological zones simultaneously experiencing compound hazard conditions. Because yield anomalies are strongly spatially synchronous across zones (r = 0.95), the expected number of concurrently affected zones increases from near zero historically (dashed line) to approximately 2.5 by the late century under SSP5-8.5.

3.4. Causal attribution of the cassava yield response

To determine whether the negative SPEI-yield relationship reflects a causal wet-stress mechanism or arises from coincident climate trends, we examined the drivers of detrended interannual cassava yield variability at the state level and applied the PCMCI+ causal-discovery algorithm[42] to the joint climate-yield record. During the historical period, cassava yield anomaly remained negatively associated with SPEI after removing temporal trends and controlling for temperature, radiation, and precipitation (partial $r = -012$) (**Figure 6a**). This result indicates that the wet-stress response represents a genuine interannual signal rather than an artefact of shared long-term trends. However, temperature was the strongest driver of year-to-year yield variability (partial $r = -0.41$), whereas the effects of SPEI and radiation were smaller and of comparable magnitude ($|\text{partial } r| \approx 0.11 - 0.12$).

In the future projections, the detrended association between SPEI and yield weakened to near zero (partial $r = -0.07$ under SSP2-4.5 and $r = -0.01$ under SSP5-8.5), whereas the negative effect of temperature persisted (partial $r = -0.23$ to -0.30). Consistent with these results, the PCMCI+ analysis across the full record identified temperature as the dominant direct causal driver of cassava yield, with a significant temperature-yield link detected in 59% of state-level time series, compared with only 13% for SPEI (**Figure 6b**). These findings indicate that the projected increase in compound low-yield/wet hazard is driven primarily by warming-related shifts in the yield distribution rather than by a stronger SPEI-yield relationship. The historical wet-stress sensitivity remains relevant but appears comparatively weak and largely stationary over time.

The model-based results were further supported by observational evidence. Across the 30 states, mean observed cassava yield during 1995-2014 was positively correlated with precipitation in the unadjusted analysis ($r = +0.56$). However, after controlling for temperature and solar radiation, the relationship remained and became strongly negative (partial $r = -0.56$). This reversal suggests that states receiving more precipitation than expected given their thermal and radiative conditions tended to have lower cassava yields. Together, the model-based and observational analyses support excess-water stress as a genuine constraint on cassava production while identifying temperature as the dominant driver of projected yield decline and the resulting increase in compound low-yield/wet hazard.

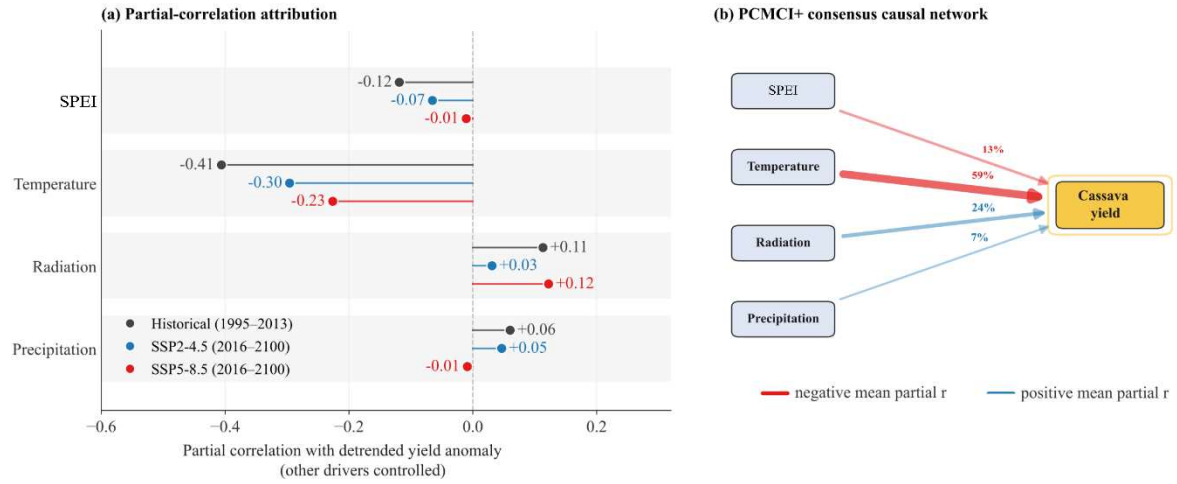


Figure 6. Causal attribution of interannual cassava yield variability. (a) Partial correlations between detrended state-level cassava yield anomalies and key hydro-climatic drivers (SPEI, Temperature, Radiation, and Precipitation), controlling for the effects of the other drivers. Coefficients are compared across the historical period (1995–2013, grey) and future projections (2016–2100) under SSP2-4.5 (blue) and SSP5-8.5 (red). Temperature remains the dominant negative driver of yield variability across all timeframes, while the historical negative sensitivity to excess wetness (SPEI) represents a genuine interannual signal that weakens toward zero in future scenarios. (b) Direct causal links between climatic drivers and cassava yield as identified by the PCMCI+ consensus causal network. Arrow thickness and the corresponding percentages denote the fraction of state-level time series exhibiting a statistically significant link, with red and blue arrows signifying negative and positive mean partial correlations, respectively. The network confirms temperature as the primary direct causal driver (significant in 59% of series), demonstrating that projected yield declines and the resulting compound hazard increases are driven primarily by warming-related shifts rather than a strengthening of the SPEI-yield relationship (13%).

4. Discussion and conclusions

This study identifies excess water, rather than drought, as an important hydro-climatic constraint on cassava production in Nigeria's predominantly humid agro-ecological environments. Across all seven agro-ecological zones, wetter-than-normal conditions were associated with lower cassava yields, while causal analysis indicated that this wet-stress signal persists after accounting for temporal trends and other major climate drivers. This challenges the dominant emphasis on drought in climate-risk assessments of major African crops and highlights the possibility that cassava risk may be underestimated when analyses focus only on water deficits or yield trends in isolation[13].

The negative relationship between SPEI and cassava yield is consistent with the hydroclimatic setting of humid Nigeria, where growing-season precipitation can frequently

exceed evapotranspiration[48]. Under such conditions, wetter-than-normal periods can increase soil saturation rather than alleviate water limitation. Although cassava is widely recognised for its drought tolerance, its storage roots remain susceptible to waterlogging[12]. Prolonged soil saturation can induce hypoxia, impair root respiration, reduce storage-root bulking and starch accumulation, and thereby reduce yield. Excess moisture can also increase the incidence of fungal and bacterial disease and accelerate post-harvest deterioration[49]. Together with the statistical and causal evidence, these mechanisms support excess-water stress as a genuine hydro-climatic constraint on cassava production in humid Nigeria.

A central contribution of this study is to explain how the compound low-yield/wet hazard emerges. The projected increase does not result primarily from progressively stronger wet stress or an intensification of the SPEI-yield dependence. Instead, the results indicate a two-stage process. First, warming progressively shifts the cassava yield distribution downward, causing an increasing number of years to fall below the historical low-yield threshold. Second, because cassava remains sensitive to excess-water stress, these increasingly frequent low-yield years can coincide with abnormally wet conditions, thereby amplifying the compound hazard. Thus, the risk increases primarily because crop vulnerability changes with warming, rather than because the SPEI-yield dependence itself become stronger.

This mechanism explains both the delayed emergence and nonlinear increase in compound risk. During the early part of the projection, simulated yields remain relatively close to or above the historical baseline, and few years cross the low-yield threshold. Consequently, compound hazard remains low despite the persistent sensitivity to wet conditions. Beyond mid-century, however, continued warming shifts the yield distribution sufficiently downward for low-yield years to become increasingly common, after which concurrent wet conditions substantially amplify the hazard. By the late century, return periods in the most affected zones fall to approximately one to two years under SSP5-8.5[50]. The concentration of risk towards the end of the century therefore reflects the interaction between changing yield distributions and persistent wet-stress sensitivity rather than an artefact arising from the analytical method.

More broadly, this finding has implications for the assessment of compound climate risk. Compound hazards can intensify substantially when the distribution of impacts shifts, even if the dependence between the climatic driver and the affected system remains broadly stationary. Risk assessments focused solely on changing climate extremes or on changes in climate–impact dependence may therefore overlook delayed and nonlinear transition in compound risk. Examining changes in the distribution of impacts is particularly important for agricultural systems, where gradual warming can progressively move crop yields across critical thresholds before climate hazards themselves undergo an equally abrupt change.

The spatial and scenario-dependent patterns further demonstrate that compound risk cannot be inferred from warming alone. Under SSP5-8.5, the largest late-century hazards occur primarily in the northern savanna zones, particularly the Sahel Savanna, where low-yield and wet conditions can become frequent. In contrast, several wetter southern zones exhibit greater compound hazard under SSP2-4.5 than under SSP5-8.5. These differences reflect interactions among temperature-induced yield changes, shifts in hydroclimatic conditions, and the historical thresholds used to define compound events. The relationship between emissions and compound risk is therefore zone-specific rather than monotonic. Adaptation strategies based solely on the highest-emission scenario could consequently overlook risks that are greater

under intermediate forcing in some regions. Climate-risk planning should instead be tailored to the climate–yield dynamics of individual agro-ecological zones.

These findings also challenge the prevailing emphasis on drought as the dominant hydro-climatic threat to African cassava and other root and tuber crops. Many assessments identify rising temperature and water deficits as the principal threats and therefore prioritise drought-tolerant varieties and supplementary irrigation[51]. Such measures remain important in semi-arid regions where cassava production is genuinely water-limited. However, transferring drought-oriented adaptation strategies directly to humid cassava systems may be inappropriate when excess water and waterlogging are more important constraints. The key implication is not that drought is irrelevant, but that climate-risk priorities must reflect agro-ecological conditions. This is consistent with broader evidence that interacting stresses can produce impacts greater than those expected from individual hazards considered separately[13].

The projected consequences for food security are potentially substantial. Under the assumptions used here, high-emission climate change could produce national cassava production shortfalls of approximately 7.8 Mt yr^{-1}, equivalent to the annual dietary energy requirements of roughly 12 million people[52]. These estimates should be interpreted as indicators of potential exposure rather than precise forecasts because they depend on climate-model uncertainty, crop-model assumptions, and socioeconomic conditions. Nevertheless, the projected transition from isolated events to frequent compound low-yield/wet years implies a potentially chronic pressure on national food supply.

This concern is amplified by the strong spatial synchronisation of cassava yield anomalies across agro-ecological zones. When poor production occurs simultaneously across large parts of the country, opportunities for domestic geographic risk pooling become limited because surplus production from unaffected zones may not be available. Systemic adaptation is therefore needed alongside farm-level interventions. Potential measures include strategic food reserves, coordinated national procurement, index-based insurance, improved storage, and regional trade arrangements capable of addressing simultaneous production shortfalls. Such measures should be designed for chronic and spatially correlated supply pressures rather than only isolated agricultural shocks.

At the production scale, the results suggest that adaptation should address both warming-related yield losses and excess-water stress. Improved field drainage, soil and water management, and the development of cassava varieties with greater tolerance to waterlogging could complement existing efforts to improve drought and heat resilience. The appropriate interventions will depend on local soils, topography, drainage capacity, and production systems. Adaptation should therefore move beyond a one-dimensional drought framework towards strategies that explicitly account for interacting heat and excess-water stresses.

Several limitations should, however, temper interpretation of the projected hazard magnitude. First, the simulations do not explicitly represent time-varying atmospheric CO concentrations. Because CO fertilisation can enhance photosynthesis and water-use efficiency in cassava, omitting this effect may underestimate future yields and overestimate late-century compound risk under the present modelling assumptions[53]. The magnitude of this response remains uncertain and may vary among cultivars. Future work should therefore incorporate transient CO forcing across a larger and more diverse CMIP6 ensemble. Until these uncertainties are better constrained, the most robust conclusion is directional: compound low-

yield/wet risk is projected to emerge after the middle of the century and intensify towards its end.

Second, the causal attribution of excess-water stress remains constrained by limited observational data and by the representation of relevant processes in the crop model. Although the PCMCI+ analysis identifies a wet-stress signal independent of temperature and radiation, causal inference remains conditional on the realism of the underlying climate–yield system[54]. Spatially detailed observed cassava yields are limited, preventing independent verification of stress sensitivities across the country. Future research should combine improved yield observations with process-based representations of waterlogging, including root aeration, anaerobic respiration, nutrient loss, pathogen interactions, and interactions between excess water and heat. Such work would help distinguish direct physiological effects from secondary consequences and provide a stronger basis for adaptation recommendations.

In addition, aggregation at the agro-ecological-zone scale may conceal important local heterogeneity in soils, topography, drainage capacity, management, and cultivar responses. These factors can strongly influence waterlogging exposure and may also affect estimates of spatial synchrony. Extending the compound-risk framework to state, local-government, or grid scales would help determine whether the high inter-zone yield correlation reflects common climate forcing or is partly influenced by spatial aggregation. More spatially explicit approaches, potentially including graph-based methods capable of representing interactions among production units and multiple climate drivers, could further improve understanding of how compound agricultural risks propagate across space, if interpretability is retained.

Overall, this study shows that cassava climate risk in humid Nigeria cannot be understood through drought alone. Excess water is an important hydro-climatic constraint, while warming progressively shifts cassava yields downward and creates the conditions under which wet years increasingly coincide with low production. The resulting compound hazard is delayed, nonlinear, and potentially chronic, emerging primarily through changes in the distribution of crop impacts rather than through strengthened climate–yield dependence. This provides a broader insight for compound-risk assessment: changes in vulnerability and impact distributions can be as important as changes in climate hazards themselves. The copula-based framework used here, which separates marginal distributions from dependence structure and accommodates changing marginals, provides a useful approach for identifying such delayed, distribution-driven risks.

Safeguarding cassava production in Nigeria will therefore require adaptation strategies that address excess-water management alongside warming-related yield decline and systemic food-security exposure. Improving spatially detailed yield observations, representing waterlogging and interacting stresses more explicitly, and evaluating transient CO_2 responses will be essential for refining the magnitude and timing of future risk. Nevertheless, the central message is already clear: in humid cassava systems, the greatest hydro-climatic risk may arise not from too little water, but from the increasing coincidence of persistently wet conditions with a crop system whose yield distribution has been progressively weakened by warming.

Acknowledgements

We gratefully acknowledge the financial support of the German Research Foundation (DFG) for the "FAIRagro" project (No. 501899475). We would also like to acknowledge the project

entitled "Supporting Agroecological Transitions of Agroforestry Landscapes using an Innovative Transdisciplinary Assessment Framework" (AGRECO4CAST). The project is co-funded by the European Union: "AGROECOLOGY Call 1- AGRECO4CAST (ID132)". Views and opinions expressed are, however, those of the author(s) only and do not necessarily reflect those of the European Union or the European Research Executive Agency (REA). Neither the European Union nor the granting authority (funding ID for Germany: 031B1610A) can be held responsible. We also acknowledge the PARAM-VC project (funding ID for Germany: 01DQ25001A), under the Indo-German Science & Technology Centre (IGSTC) 2+2 call, funded jointly by the Department of Science and Technology (DST) under the Government of India and the Federal Ministry of Research, Technology and Space of Germany (BMFTR), LL-SYSTAIN (Grant Labs-2024-IÖR), and "SUSTAINCrop" (HORIZON-EUROPE, funding ID: 0672EMSM).

References

1. Rathore, L. S., Kumar, M., Moftakhari, H. & Ganguli, P. Divergent changes in crop yield loss risk due to droughts over time in the US. *Environ. Res. Lett.* **19**, 114008 (2024).
2. Van Loon, A. F. *et al.* Review article: Drought as a continuum – memory effects in interlinked hydrological, ecological, and social systems. *Nat. Hazards Earth Syst. Sci.* **24**, 3173–3205 (2024).
3. Hazaymeh, K., K. Hassan, Q., & 1 Department of Geomatics Engineering, Schulich School of Engineering, University of Calgary, 2500 University Drive NW, Calgary, Alberta, Canada T2N 1N4. Remote sensing of agricultural drought monitoring: A state of art review. *AIMS Environmental Science* **3**, 604–630 (2016).
4. Mishra, A. K. & Singh, V. P. A review of drought concepts. *Journal of Hydrology* **391**, 202–216 (2010).
5. Parmar, A., Sturm, B. & Hensel, O. Crops that feed the world: Production and improvement of cassava for food, feed, and industrial uses. *Food Sec.* **9**, 907–927 (2017).
6. Sivamani, S. *et al.* Evaluation of the potential of cassava-based residues for biofuels production. *Reviews in Environmental Science and Bio/Technology* **17**, 553–570 (2018).
7. Akinwumiju, A. S., Adelodun, A. A. & Orimoogunje, O. I. Agro-Climato-Edaphic Zonation of Nigeria for a Cassava Cultivar using GIS-Based Analysis of Data from 1961 to 2017. *Sci Rep* **10**, 1259 (2020).
8. Sultan, B. & Gaetani, M. Agriculture in West Africa in the Twenty-First Century: Climate Change and Impacts Scenarios, and Potential for Adaptation. *Front. Plant Sci.* **7**, (2016).
9. Mereu, V., Carboni, G., Gallo, A., Cervigni, R. & Spano, D. Impact of climate change on staple food crop production in Nigeria. *Climatic Change* **132**, 321–336 (2015).
10. Mckee, T., Doesken, N. & Kleist, J. THE RELATIONSHIP OF DROUGHT FREQUENCY AND DURATION TO TIME SCALES. in (1993).
11. Vicente-Serrano, S. M., Beguería, S. & López-Moreno, J. I. A Multiscalar Drought Index Sensitive to Global Warming: The Standardized Precipitation Evapotranspiration Index. *Journal of Climate* **23**, 1696–1718 (2010).
12. Howeler, R., Lutaladio, N. & Thomas, G. *Save and Grow: Cassava a Guide to Sustainable Production Intensification*. (FAO, Rome, 2013).

13. Zscheischler, J. *et al.* Future climate risk from compound events. *Nature Clim Change* **8**, 469–477 (2018).
14. Chen, J. *et al.* Bias correcting climate model multi-member ensembles to assess climate change impacts on hydrology. *Climatic Change* **153**, 361–377 (2019).
15. Copernicus Climate Change Service. ERA5-Land hourly data from 1950 to present. Copernicus Climate Change Service (C3S) Climate Data Store (CDS) https://doi.org/10.24381/CDS.E2161BAC (2019).
16. FAO. FAOSTAT Statistical Database. *Food and Agricultural Organization of the UN* (2010).
17. Chude, V. O., Olayiwola, S. O., Daudu, C. & Ekeoma, A. *Fertilizer Use and Management Practice for Crops in Nigeria*. (Federal Fertilizer Department, Federal Ministry of Agriculture and Rural Development, Abuja, 2012).
18. *Handbook of Hydrology*. (McGraw-Hill, New York, 1995).
19. Thrasher, B. *et al.* NASA Global Daily Downscaled Projections, CMIP6. *Sci Data* **9**, 262 (2022).
20. Swart, N. C. *et al.* The Canadian Earth System Model version 5 (CanESM5.0.3). *Geosci. Model Dev.* **12**, 4823–4873 (2019).
21. Hajima, T. *et al.* Development of the MIROC-ES2L Earth system model and the evaluation of biogeochemical processes and feedbacks. *Geosci. Model Dev.* **13**, 2197–2244 (2020).
22. Mauritsen, T. *et al.* Developments in the MPI-M Earth System Model version 1.2 (MPI-ESM1.2) and Its Response to Increasing CO_2. *J Adv Model Earth Syst* **11**, 998–1038 (2019).
23. Seland, Ø. *et al.* Overview of the Norwegian Earth System Model (NorESM2) and key climate response of CMIP6 DECK, historical, and scenario simulations. *Geosci. Model Dev.* **13**, 6165–6200 (2020).
24. Faye, A. & Akinsanola, A. A. Evaluation of extreme precipitation indices over West Africa in CMIP6 models. *Clim Dyn* **58**, 925–939 (2022).
25. Monerie, P.-A., Wainwright, C. M., Sidibe, M. & Akinsanola, A. A. Model uncertainties in climate change impacts on Sahel precipitation in ensembles of CMIP5 and CMIP6 simulations. *Clim Dyn* **55**, 1385–1401 (2020).
26. Gaiser, T. *et al.* Modeling biopore effects on root growth and biomass production on soils with pronounced sub-soil clay accumulation. *Ecological Modelling* **256**, 6–15 (2013).
27. Enders, A. *et al.* SIMPLACE—a versatile modelling and simulation framework for sustainable crops and agroecosystems. *in silico Plants* **5**, diad006 (2023).
28. Van Ittersum, M. K. *et al.* Yield gap analysis with local to global relevance—A review. *Field Crops Research* **143**, 4–17 (2013).
29. Resop, J. P., Fleisher, D. H., Timlin, D. J. & Reddy, V. R. Biophysical Constraints to Potential Production Capacity of Potato across the U.S. Eastern Seaboard Region. *Agronomy Journal* **106**, 43–56 (2014).
30. Li, Z. *et al.* Optimizing Wheat Yield, Water, and Nitrogen Use Efficiency With Water and Nitrogen Inputs in China: A Synthesis and Life Cycle Assessment. *Front. Plant Sci.* **13**, 930484 (2022).

31. Kiniry, J. R., Tischler, C. R. & Van Esbroeck, G. A. Radiation use efficiency and leaf CO2 exchange for diverse C4 grasses. *Biomass and Bioenergy* **17**, 95–112 (1999).
32. Soltani, A., Robertson, M. J., Rahemi-Karizaki, A., Poorreza, J. & Zarei, H. Modelling Biomass Accumulation and Partitioning in Chickpea (*Cicer arietinum* L.). *J Agronomy Crop Science* **192**, 379–389 (2006).
33. Wolf, J. *User Guide for LINTUL5: Simple Generic Model for Simulation of Crop Growth under Potential, Water Limited and Nitrogen, Phosphorus and Potassium Limited Conditions.* (Wageningen University, Netherlands, 2012).
34. Addiscott, T. M. & Whitmore, A. P. Simulation of solute leaching in soils of differing permeabilities. *Soil Use and Management* **7**, 94–102 (1991).
35. Ezui, K. S., Leffelaar, P. A., Franke, A. C., Mando, A. & Giller, K. E. Simulating drought impact and mitigation in cassava using the LINTUL model. *Field Crops Research* **219**, 256–272 (2018).
36. Srivastava, A. K. *et al.* Cassava yield gap—A model-based assessment in Nigeria. *Front. Sustain. Food Syst.* **6**, 1058775 (2023).
37. Kim, D. & Rhee, J. A drought index based on actual evapotranspiration from the Bouchet hypothesis. *Geophysical Research Letters* **43**, (2016).
38. Zhang, X. *et al.* Assessment of an Evapotranspiration Deficit Drought Index in Relation to Impacts on Ecosystems. *Adv. Atmos. Sci.* **36**, 1273–1287 (2019).
39. Sun, T., Cheng, Y. & Ding, Y. An Information Ratio-Based Goodness-of-Fit Test for Copula Models on Censored Data. *Biometrics* **79**, 1713–1725 (2023).
40. Ayantobo, O. O., Li, Y. & Song, S. Multivariate Drought Frequency Analysis using Four-Variate Symmetric and Asymmetric Archimedean Copula Functions. *Water Resour Manage* **33**, 103–127 (2019).
41. Hawkins, E. & Sutton, R. The potential to narrow uncertainty in regional climate predictions. *Bulletin of the American Meteorological Society* **90**, 1095–1107 (2009).
42. Runge, J. *et al.* Identifying causal gateways and mediators in complex spatio-temporal systems. *Nature Communications* **10**, 2553 (2019).
43. *Human Energy Requirements: Report of a Joint FAO/WHO/UNU Expert Consultation Rome, 17 - 24 October 2001*. (Food and Agricultural Organization of the United Nations, Rome, 2004).
44. International Fund for Agricultural Development & Food and Agriculture Organization. A Review of Cassava in Africa with Country Case Studies on Nigeria, Ghana, United Republic of Tanzania, Uganda and Benin. in *Proceedings of the Validation Forum on the Global Cassava Strategy* vol. 2 (International Fund for Agricultural Development (IFAD), Rome, Italy, 2025).
45. Esiobu, N. S. *et al.* WHAT DRIVES CASSAVA FARMERS' OUTPUT MAXIMIZATION POTENTIALS? EMPIRICAL EVIDENCE FROM IMO STATE, NIGERIA. https://doi.org/10.5281/ZENODO.18671896 (2026) doi:10.5281/ZENODO.18671896.
46. Bayata, A. Review on nutritional value of cassava for use as a staple food. *Science Journal of Analytical Chemistry* **7**, 83–91 (2019).
47. Newby, J. C. & Le, T. C. T. *Cassava Market Update and Short-Term Outlook*. http://www.rtb.cgiar.org (2018).

48. Adefolalu, D. O. Precipitation trends, evapotranspiration and the ecological zones of Nigeria. *Theor Appl Climatol* **39**, 81–89 (1988).
49. Hillocks, R. & Wydra, K. Bacterial, Fungal and Nematode Diseases. *Cassava: Biology, Production and Utilization* (2002).
50. Ogunrinde, A. T. *et al.* Effects of climate change and drought attributes in Nigeria based on RCP 8.5 climate scenario. *Physics and Chemistry of the Earth, Parts A/B/C* **129**, 103339 (2023).
51. Pushpalatha, R. & Gangadharan, B. Is Cassava (Manihot esculenta Crantz) a Climate 'Smart' Crop? A Review in the Context of Bridging Future Food Demand Gap. *Tropical Plant Biology* **13**, 201–211 (2020).
52. Ikuemonisan, E. S. & Akinbola, A. E. Future Trends in Cassava Production: Indicators and its Implications for Food Supply in Nigeria. *AJAEES* 60–74 (2021) doi:10.9734/ajaees/2021/v39i330546.
53. Anyaegbu, C. N. *et al.* Impact of Climate Change on Cassava Yield in Nigeria: An Autoregressive Distributed Lag Bound Approach. *Agriculture* **13**, 80 (2022).
54. Sowunmi, F. A., Adeyemi, O. T. & Bello, A. A. Effects of climatic variability on cassava production in Nigeria. *J. Agribus. Rural Dev.* **57**, 327–335 (2020).

822 **Supplementary table S1**: Cassava crop parameter

Name	Description	Unit	Value
Crop parameters			
TSUM1	Temperature sum from emergence to anthesis	°C day-1	2275
TSUM2	Temperature sum from anthesis to maturity	°C day-1	3300
TBASEM	Lower threshold temperature for emergence	°C	15.0
TEFFMX	Maximum effective temperature for emergence	°C	30.0
TSUMEM	Temperature sum from sowing to emergence	°C	160.0
RUE-0.0	Radiation use efficiency at development stage 0	g MJ-1	2.0
RUE-1.0	Radiation use efficiency at development stage 1.0	g MJ-1	1.2
RUE-1.3	Radiation use efficiency at development stage 1.3	g MJ-1	1.2
RUE-2.0	Radiation use efficiency at development stage 2.0	g MJ-1	1.2
SLATB-0.0	Specific leaf area at development stage 0	m2 g-1	0.012
SLATB-1.02	Specific leaf area at development stage 0.9	m2 g-1	0.012
SLATB-1.33	Specific leaf area at development stage 1.0	m2 g-1	0.012
SLATB-2.0	Specific leaf area at development stage 2.0	m2 g-1	0.01
LAI critical	Critical leaf area beyond which leaves die due to self shading	m2 m-2	3.5
RGRLAI	Maximum relative increase in LAI	ha ha-1 day-1	0.01
RDI	Initial rooting depth	m	0.1
RDMCR	Maximum rooting depth	m	1.8
RRI	Maximum daily increase in rooting depth	m	0.012
TDWI	Initial total crop dry weight	kg ha-1	3.5

823